



Exploring movement and energy in human P-glycoprotein conformational rearrangement

Yue Zhang, Weikang Gong, Yan Wang, Yang Liu & Chunhua Li

To cite this article: Yue Zhang, Weikang Gong, Yan Wang, Yang Liu & Chunhua Li (2019) Exploring movement and energy in human P-glycoprotein conformational rearrangement, *Journal of Biomolecular Structure and Dynamics*, 37:5, 1104-1119, DOI: [10.1080/07391102.2018.1461133](https://doi.org/10.1080/07391102.2018.1461133)

To link to this article: <https://doi.org/10.1080/07391102.2018.1461133>



[View supplementary material](#) 



Accepted author version posted online: 05
Apr 2018.
Published online: 24 Apr 2018.



[Submit your article to this journal](#) 



Article views: 80



[View Crossmark data](#) 



Exploring movement and energy in human P-glycoprotein conformational rearrangement

Yue Zhang^a, Weikang Gong^a, Yan Wang^b, Yang Liu^a and Chunhua Li^{a*}

^aCollege of Life Science and Bioengineering, Beijing University of Technology, Beijing, 100124, China; ^bKey Laboratory of Molecular Biophysics of the Ministry of Education, School of Life Science and Technology, Huazhong University of Science and Technology, Wuhan, Hubei, 430074, China

Communicated by Ramaswamy H. Sarma

(Received 17 October 2017; accepted 27 March 2018)

Human P-glycoprotein (P-gp), a kind of ATP-Binding Cassette transporter, can export a diverse variety of anti-cancer drugs out of the tumor cell. Its overexpression is one of the main reasons for the multidrug resistance (MDR) of tumor cells. It has been confirmed that during the substrate transport process, P-gp experiences a large-scale structural rearrangement from the inward- to outward-facing states. However, the mechanism of how the nucleotide-binding domains (NBDs) control the transmembrane domains (TMDs) to open towards the periplasm in the outward-facing state has not yet been fully characterized. Herein, targeted molecular dynamics simulations were performed to explore the conformational rearrangement of human P-gp. The results show that the allosteric process proceeds in a coupled way, and first the transition is driven by the NBDs, and then transmitted to the cytoplasmic parts of TMDs, finally to the periplasmic parts. The trajectories show that besides the translational motions, the NBDs undergo a rotation movement, which mainly occurs in *xy* plane and ensures the formation of the correct ATP-binding pockets. The analyses on the interaction energies between the six structure segments (cICLs) from the TMDs and NBDs reveal that their subtle energy differences play an important role in causing the periplasmic parts of the transmembrane helices to separate from each other in the established directions and in appropriate amplitudes. This conclusion can explain the two experimental phenomena about human P-gp in some extent. These studies have provided a detailed exploration into human P-gp rearrangement process and given an energy insight into the TMD reorientation during P-gp transition.

Keywords: human P-glycoprotein; targeted molecular dynamic simulation; conformational rearrangement; movement coupling; interaction energy

Introduction

The emergence of multidrug resistance (MDR) is an increasingly important problem in treatment of some diseases (Bera et al., 2017; Dwivedi et al., 2018; Kesherwani, Michael, Fukui, & Velmurugan, 2017; Pandey et al., 2018). P-glycoprotein (P-gp), a member of the ATP-Binding Cassette (ABC) transporter protein superfamily, can export substrates across the cell membrane utilizing the energy of ATP binding and hydrolysis. Human P-gp, with broad substrate specificity, can pump a wide variety of anti-cancer drugs out of the cell, leading to a decrease in intracellular drug concentration, which is one of the major reasons for MDR of tumor cells (Gutmann, Ward, Urbatsch, Chang, & van Veen, 2010; Manoharan, Chennoju, & Ghoshal, 2018; Manoharan & Ghoshal, 2017; Shahrazi et al., 2018a). Biochemical studies have confirmed that human P-gp undergoes a large-scale conformational rearrangement to export anti-cancer drugs out of the cells (Dawson & Locher, 2006). Thus, to inhibit P-glycoprotein-mediated drug transport,

it is very important to understand the rearrangement mechanism of human P-gp.

Human P-glycoprotein is a 170 kDa single chain protein with two pseudosymmetrical halves (Klepsch & Ecker, 2010), each composed of one nucleotide-binding domain (NBD) and one transmembrane domain (TMD) (Higgins & Linton, 2004). The NBDs are highly conserved in structure and sequence among all ABC transporters, which can be attributed to their same function: ATP binding and hydrolysis (ter Beek, Guskov, & Slotboom, 2014). By contrast, the sequences and architectures of the TMDs are considerably variable, which reflects the chemical diversity of the translocated substrates.

Figure 1 shows the structural models of human P-gp in inward-facing (IF) and outward-facing (OF) states. Each TMD is composed of six transmembrane (TM) helices that are connected by intracellular helices (IHs) in the cytoplasm and extracellular loops (ELs) in the periplasm. Cytoplasmic parts of TM helices usually are

*Corresponding author. Email: chunhuali@bjut.edu.cn

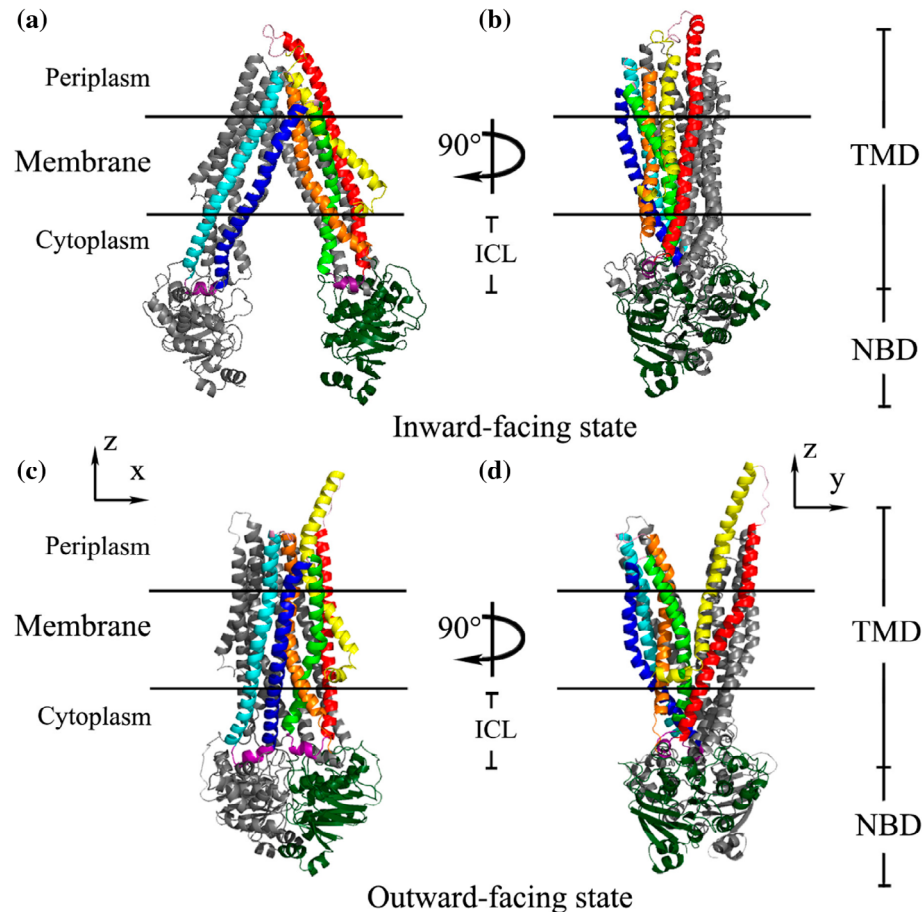


Figure 1. Three-dimensional structural models of human P-gp in the inward-facing conformation (a) and (b) and the outward-facing conformation (c) and (d). Horizontal bars stand for the approximate position of the lipid bilayer. The C-terminal half of P-gp is given in gray and the N-terminal half in colors: TM helices 1–6 shown in yellow, red, green, blue, cyan and orange respectively, and IHLs and ELs in purple and pink, respectively.

defined as intracellular loops (ICLs). For NBDs, its dimer interface consists of two ATP-binding pockets, each formed by the Walker A, Walker B, H-loop, Q-loop, A-loop of one NBD and D-loop and the conserved ABC-signature motif LSGQQ of the other (Pan & Aller, 2015; Sauna & Ambudkar, 2007). The ATP is sandwiched between them, forming an ATP-sandwich structure (Sauna & Ambudkar, 2007). Recently, biochemical, structural, and genetic studies have led to the ATP-switch model for ABC transporters (Linton & Higgins, 2007). According to this model, the transport process can be described as follows. First, the binding of ATP to the NBDs induces the dimerization of the two NBDs to form the ATP-sandwich structure, and the TMDs flip from facing inward to facing outward at same time, presenting the substrate to the extracellular side. Then the ATP hydrolysis drives the NBD dimer dissociation to reset the TMDs to the inward facing, completing the cycle. Although this model can generally describe the transport

process, more details about the conformational rearrangement are needed to investigate for a deeper understanding of the P-gp transport mechanism.

Experimental researches on human P-gp have mainly focused on inhibitor development, in order to block this efflux mechanism and then restore chemotherapeutics efficacy (Katayama et al., 2015; Kort, Sparidans, Wagenaar, Beijnen, & Schinkel, 2015; Tsujimura, Saito, Nawata, Nakayamada, & Tanaka, 2008). It is very difficult for experimental methods to obtain the dynamic information at the atomic level about the large-scale conformational rearrangement mainly due to the transients of intermediate conformations and the difficulty of obtaining the transmembrane protein samples. Theoretically, the conventional and enhanced sampling molecular dynamics (MD) simulations provide useful tools at the atomic level to analyze the structural, mechanical and thermodynamic properties of biomolecules. The targeted MD and steered MD methods can additionally explore

the process of large-scale conformational rearrangements of proteins. McCormick et al. utilized docking and targeted MD simulations to study the transport pathways of different anti-cancer drugs through human P-gp (McCormick, Vogel, & Wise, 2015). Using multi-targeted molecular dynamics method, Prajapati and Sangamwar explored the conformational changes occurring in TMDs during the catalytic cycle of ATP hydrolysis (Prajapati & Sangamwar, 2014). In order to research the catalytic mechanism of P-gp, Wise applied targeted MD simulation technique to elucidate catalytically relevant structures of P-gp (Wise, 2012). Still with the targeted MD simulations, Chang et al. investigated the molecular mechanism in the conformational transmission of human P-gp from the NBDs to the TMDs (Chang, Liu, Dong, & Sun, 2013). From the works above, the current studies have provided some insight into the conformational rearrangement process of P-gp, as well as the transport pathways of anti-cancer drugs through P-gp, while the mechanism by which the NBDs control the opening of TMDs towards the periplasm in the outward-facing state has not yet been fully characterized.

In this paper, the targeted MD simulation technology was performed to simulate the conformational rearrangement process from IF to OF state of human P-gp. We analyzed the movements of the NBDs and TMDs, and the interaction energies and movement coupling between them during the conformational rearrangement process from the IF to OF states. We explored the physical mechanism of the reorientation of TMDs to the periplasmic side.

Materials and methods

Homology modeling of the inward-facing state of human P-gp

The experimental structure of human P-gp in the IF conformation has not been resolved. We constructed the three-dimensional structure of this conformation using the homology modeling software Modeller 9.14 (Eswar, Eramian, Webb, Shen, & Sali, 2008; Sanchez & Sali, 2000). The crystal structure of mouse P-gp in the IF state (PDB ID: 4Q9H resolved at 3.4 Å) was selected as the template, which has 87% and 93% sequence identity and similarity with human P-gp, respectively. The sequence of human P-gp was obtained from NCBI database (accession code: NP_000918.2 [Chen et al., 1986; Gekeler, Weger, & Probst, 1990; Kioka et al., 1989]). Because of the missing structure segments (residue 1 to 29, 627 to 688, and 1274 to 1275) in the IF structure of mouse P-gp, the corresponding sequence segments (residue 1 to 29, 631 to 692 and 1278 to 1279) in human P-gp were removed when its structure was built. First, fifty models were constructed by Modeller 9.14 and then opti-

mized with the method of conjugate gradients. Afterward, simulated annealing MD simulations were used to refine these structures and the best model was selected based on the values of the Modeller objective function and the DOPE assessment scores (Shen & Sali, 2006). Then, the structure quality of this best model was evaluated by Ramachandran plot (Kolaskar & Sawant, 1996) generated from PROCHECK program (Laskowski, MacArthur, Moss, & Thornton, 1993). To make sure the IF structure has the same residues with the OF one, their common residues were remained and thus the residue 30 to 36, 694 to 699 and 1277 in the IF structure were removed.

Simulation systems

The human P-gp structures in the IF and OF states are respectively from the structure generated through homology modeling in this study, and the model obtained by O'Mara's group (O'Mara & Tielemans, 2007) which has been widely used in a number of theoretical studies (Binkathlán & Lavasanifar, 2013; Eckford & Sharom, 2009; Locher, 2008; Loo & Clarke, 2008; Matsson, Pedersen, Norinder, Bergström, & Artursson, 2009; Mornon, Lehn, & Callebaut, 2008; Seeger & van Veen, 2009). The simulation systems with IF and OF states were built using the following methods. First, the protein was vertically buried into a POPC bilayer membrane (140 Å × 140 Å) by VMD software. The orientation of the protein conformation was properly adjusted with respect to membranes based on the information from the Orientations of Proteins in Membranes (OPM) database (Lomize, Lomize, Pogozheva, & Mosberg, 2006). The IF conformation opens towards the negative z direction and OF conformation opens to the positive z direction. The x axis is directed along the straight line connecting the geometric centers of the two NBDs in the IF state. Here, like Chang's work on P-gp conformational transition (Chang et al., 2013), we also used the cartesian coordinates (not internal ones) to describe the movements of NBDs and TMDs because of the complexity of their motions. The POPC molecules overlapping with proteins were removed by VMD software. Then, water molecules were added into the systems, and to neutralize the system and maintain a physiological ionic concentration, Na⁺ and Cl⁻ ions were also added to the system at a concentration of 150 mM. The final system with IF conformation contains 319,162 atoms including 78,972 water molecules and 474 POPC lipid molecules in a rectangular box (140 Å × 140 Å × 180 Å). For the simulation system with outward-facing conformation, the total number of atoms is 333,598 in a similar sized rectangular box with 83,507 water molecules and 479 POPC lipid molecules.

Molecular dynamic simulations

MD simulations were carried out using the NAMD 2.10 package (Phillips et al., 2005) and CHARMM force field (Feller, Yin, Pastor, & MacKerell, 1997; MacKerell et al., 1998). First for the two systems, POPC bilayer molecules were minimized for 5000 steps and then equilibrated for 0.5 ns with other atoms fixed. Then, the whole system was minimized for 20,000 steps and then equilibrated for 3.0 ns with only protein C α atoms constrained. The keep_water_out.tcl script (<http://www.ks.uiuc.edu/Research/namd/>) was used to prevent water molecules entering into the membrane hydrophobic region in a frequency of every 200 fs. Finally, the final equilibrium structures were used as the initial and targeted structures for targeted MD simulations.

The equilibration simulations were performed in the NPT ensemble with periodic boundary conditions. The temperature was set to 310 K and kept constant during the simulation process using a Langevin thermostat with a damping coefficient of 1.0 ps⁻¹ (Weng, Fan, & Wang, 2010). The pressure was kept at 1.0 atm using the Langevin piston Nosé-Hoover method with a piston period of 200 fs and a decay time of 50 fs (Hoover, 1985; Nosé, 1984). The switching function was used for the electrostatic and van der Waals interactions, which makes the interaction shift smoothly to zero between 10 and 12 Å. The long-range electrostatic interactions were handled by the ParticleMesh Ewald (PME) method with a grid spacing of 1.0 Å (Essmann et al., 1995). In equilibration process and conventional MD simulations, the SHAKE algorithm was used to constrain all hydrogen atom-containing bonds, which allows use of a time step of 2 fs (Vangunsteren & Berendsen, 1977).

Targeted MD simulation

Targeted MD simulation, a kind of non-equilibrium simulation technique (Compoint, Picaud, Ramseyer, & Girardet, 2005; Schlitter, Engels, Krüger, Jacoby, & Wollmer, 1993), has been used to study the conformational transition and reaction pathway of biomolecules for several years (Kamerlin, Rucker, & Boresch, 2006; Kong, Ma, Karplus, & Lipscomb, 2006; Ma, Sigler, Xu, & Karplus, 2000; Wang, Hong, Paterson, Pu, & Laughlin, 2014; Xiao et al., 2015; Zhong & Guo, 2009). Targeted MD drives a structure to the target using an external potential which can be described as:

$$U_{TMD} = \frac{1}{2N} [RMSD(t) - RMSD^*(t)]^2, \quad (1)$$

where k is the force constant and N is the number of the targeted atoms. RMSD(t) is the instantaneous best-fit root mean square deviation (RMSD) of the current coordinates from the targeted coordinates. And RMSD*(t) is

the prescribed RMSD value for the current step, which changes linearly from the initial RMSD at the first Targeted MD step to the final RMSD at the last step.

In this work, the equilibrated conformations of the IF and OF states were chosen as the initial and targeted structures, respectively. The integration step is 1 fs. Refer to the work of Chang and coworkers (Chang et al., 2013), the values of the force constant k and the number of targeted atoms N are set to 1171 kcal/(mol Å²) and 1171 (all the C α atoms of human P-gp), respectively, which means the external forces were applied to all the C α atoms in the initial conformation. In addition, the values of RMSD*(t) decreased from 14.0 to 0 Å monotonically. Keep_water_out.tcl script was also used to prevent water molecules entering into the membrane hydrophobic region at a frequency of every 100 fs. To ensure the molecular allosteric mechanism is intrinsic character rather than the stochastic output of targeted MD simulations, 4 targeted MD simulations of 10 ns were carried out from the initial structure to the targeted structure under different initial conditions by assigning different initial velocities on each atom of the simulation systems.

Cross-correlation between residue displacement vectors

The cross-correlation of displacement vectors between the i th and j th residues is calculated across all C α atoms of human P-gp according to the following formula:

$$C_{ij} = \frac{(\Delta r_i \cdot \Delta r_j)}{\sqrt{(\Delta r_i \cdot \Delta r_i)(\Delta r_j \cdot \Delta r_j)}}, \quad (2)$$

where Δr_i and Δr_j are respectively the displacements of the i th and j th residues between two conformations along the allosteric pathway (Ichiye & Karplus, 1991). The cross-correlation value ranges from -1 to 1. The positive values represent that the residues move in the same direction and the negative values represent that they move in the opposite direction.

Selection of the contact segments in TMDs with NBDs and data analyses

In order to explore the energy coupling between the NBDs and TMDs, we selected those residue segments in ICLs as the contact ICLs (cICLs) with NBDs in which every residue is within 4.0 Å distance from NBDs among more than 99.5% conformations (every 500 fs 1 sample) along the targeted MD trajectories. And then the non-bonded interaction energies including van der Waals (vdW) and electrostatic (Ele) energies between cICLs and NBDs were calculated with Energy package of NAMD 2.10 with CHARMM force field. The short-range vdW interactions were calculated using the switch-

ing function, with a twin range cutoff of 10.0 and 12.0 Å. Long-range electrostatic interactions were calculated with the PME method with a cut-off of 12.0 Å. Movements of the trajectories were analyzed using VMD 1.9.1 software (Humphrey, Dalke, & Schulten, 1996). The structures for most of the following analyses were sampled every 0.2 ns. The analyses and figures are based on the average of 4 trajectories of 10 ns targeted MD simulations, and the standard deviations are shown as error bars in figures.

Results and discussion

Evaluation of homology modeling of human P-gp in the IF state

We constructed the three-dimensional structure of human P-gp in IF state using homology modeling method, as shown in Figure 1 (upper panel). The structure in OF state (lower panel in Figure 1) comes from the modeled one by O'Mara's group (O'Mara & Tielemans, 2007) with the OF state of *Staphylococcus aureus* Sav1866 as the template. Due to the absence of the experimental structure of human P-gp in IF state, we used the IF structure of mouse P-gp as the template to build the corresponding one of human P-gp. Thus, from Figure 1, the modeled IF state is a little different from the OF state mainly in the secondary structures of the periplasmic parts around EL1 region (TM1-EL1-TM2) of TM helices, while their vast majority of the second structures are the same. Furtherly, to evaluate the accuracy of the modeled structure, Ramachandran plot was calculated, as shown in Figure S1. It displays that 93.2% residues are in the favorable regions, and 99.5% residues in the acceptable regions of Ramachandran plot. A high-quality model usually has not less than 90% of residues in favorable regions. Therefore, the homology model of human P-gp established here was used for the rearrangement simulations by the targeted MD method. The PDB files of the modeled initial (IF) structure as well as the targeted (OF) one from O'Mara's group were provided in the Supplemental Files.

Conformational transition of the NBDs

As we know, this conformational transition is triggered by the movements of NBDs. Therefore, it is critical to elucidate the movements of NBDs. Before exploring the interdomain movements in NBDs, we analyzed the intradomain structural changes. Supplementary Figure S2 shows the RMSDs (all atoms) of each NBD from the corresponding one in the initial state after they are superimposed as a function of time. From Figure S2, during the first 0.8 ns mainly due to the perturbations of the external force on protein C α atoms, the RMSD value has

a small increase with 2.1 Å for NBD1 and 1.9 Å for NBD2, and then the value maintains a relatively stable equilibrium until 8.5 ns. In the last 1.5 ns, the RMSD values increase a little, which is mainly because of the small structural adjustment after the two NBDs are close enough to each other. Based on the analyses above, the internal structural changes in each NBD are very small, consistent with the results of Liu *et al.* obtained by biochemical studies (Liu & Sharom, 1997). This means that we can treat NBDs approximately as rigid bodies and use their geometric centers to analyze the relative translation movements between them.

The following analyses are about the interdomain movement between the two NBDs. Figure 2(a) gives the displacements of both NBDs in x , y , and z axes. From Figure 2(a), NBD1 moves along negative x and y directions, NBD2 moves in positive x and y directions, and they hardly move in z axis. The relative displacements between them mainly happen along x direction, with the interdomain distance in x direction declining from the initial 60–28 Å in the first 8.5 ns. Interestingly, the distance in y direction has a slight increase from 0 to 13 Å during the same period. Although the distance in y direction is increasing, the distance between geometric centers of two NBDs is still decreasing. The details on the distance changes in each direction are shown in Figure S3. It should be pointed out that the geometric centers of the two NBDs are almost the same with the mass centers of them during the simulation, which can be found by comparing Figure 2(a) with Figure S4, which give the displacements of NBDs based on geometric centers and mass centers, respectively. Therefore, we used the geometric centers of two NBDs to analyze the relative translation movements between them.

Besides the translation movement, a rotation movement between the two NBDs is also observed during the conformational rearrangement. Figure 2(b) gives the change of the angle θ formed between the two lines A and B respectively connecting residue pairs Val437-Val504 in NBD1 and Val1080-Val1146 in NBD2 during the conformational transition. From Figure 2(b), the angle θ decreases from 30° to 6° in the first 7 ns, and then maintains around 6°, which indicates that an obvious rotation occurs between the NBDs at the beginning of the rearrangement process and ends earlier than the translation movement does. The phenomenon of rotation movement between NBDs was also confirmed in other studies for ABC transporters (Chen, Lu, Lin, Davidson, & Quiocho, 2003; Furuta, Yamaguchi, Kato, & Sakurai, 2014; Moradi & Tajkhorshid, 2013; Smith *et al.*, 2002). Refer to the works (Chen *et al.*, 2003; Furuta *et al.*, 2014; Moradi & Tajkhorshid, 2013; Smith *et al.*, 2002), here the rotation movement was analyzed in xy and yz planes. The angle θ was projected onto the xy plane to form angle α (Figure 2(c) and (d)) and onto the yz plane

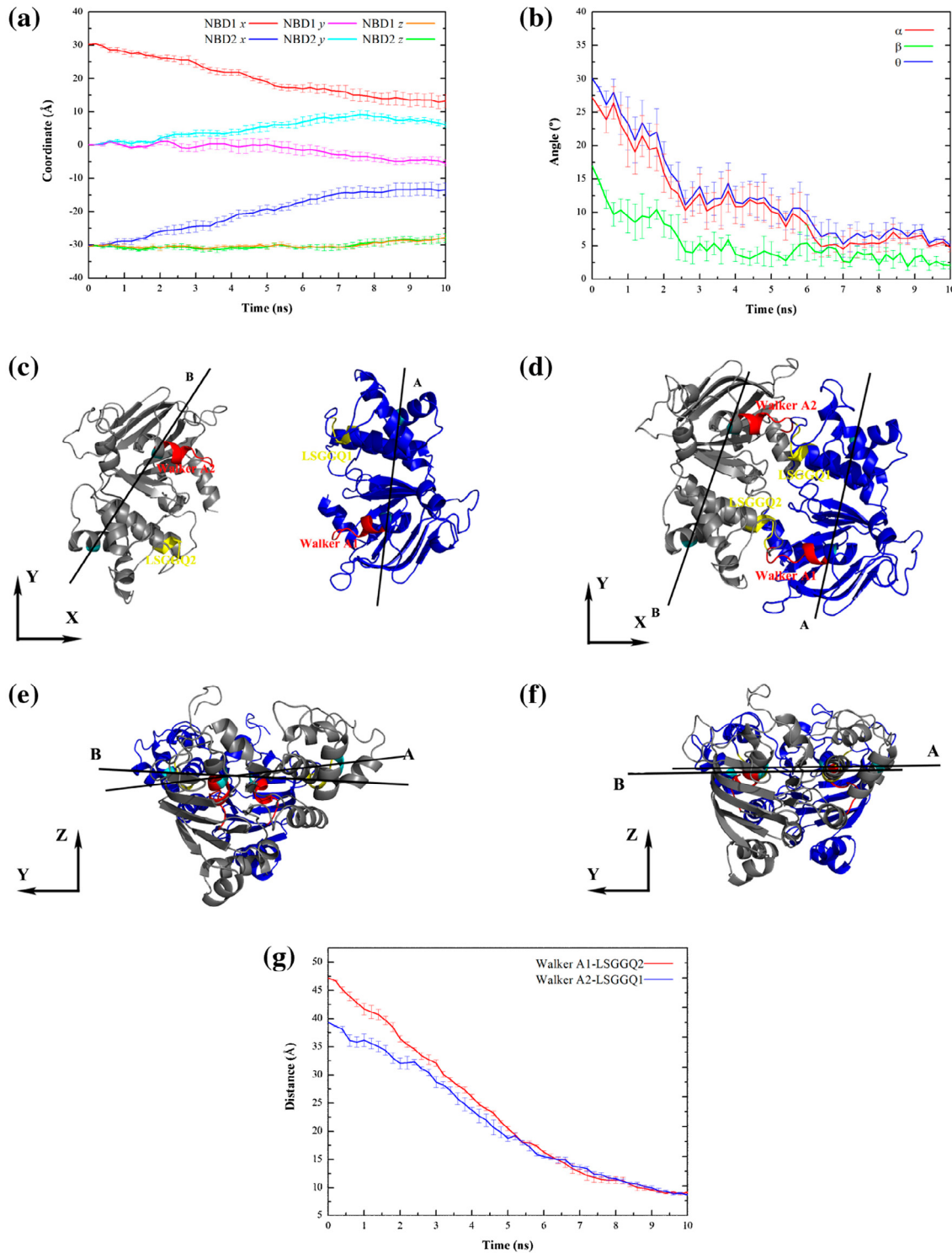


Figure 2. Translation and rotation movements of NBDs during the conformational rearrangement. (a) the translation movement of both NBDs along x , y and z directions. (b) the rotation movement between NBDs described by the change of the angle θ formed between the two lines A and B respectively connecting residue pairs Val437-Val504 and Val1080-Val1146. The angles α and β are the projection of the angle θ in xy plane and yz plane, respectively. (c), (d) and (e), (f) are the top and side views of the initial and targeted conformations of NBDs, respectively. (g) the changes of the distances between Walker A1 and LSGGQ2, Walker A2 and LSGGQ1. NBD1 and NBD2 in (c), (d), (e) and (f) are displayed in blue and grey, respectively. The Walker As and LSGGQs are colored in red and yellow, respectively.

to form angle β (Figure 2(e) and (f)), respectively. Their changes are also shown in Figure 2(b). The angle α has a 22° decrease from 27° to 5° during the simulation, while the decline of the angle β is only about 12° , which indicates that the rotation movement between NBDs happens mainly in the xy plane. We think the rotation movement between NBDs is very important for the correct formation of ATP-binding pockets. Figure 2(g) gives the changes of the distances between Walker As and signature motifs LSGGQs (forming the ATP-binding pockets, Figure 2(c) and (d)) during this process. Evidently, it is because of the rotation movement, that the distance between Walker A1 and LSGGQ2 diminishes faster than that between Walker A2 and LSGGQ1, and finally both the distances reach the same value 9 \AA . Therefore, the rotation movement is very important for ensuring the nearly simultaneous formation of the two ATP-binding pockets. Additionally, the translation movement of NBDs along x and y directions pulls Walker As and LSGGQs close to each other, also playing an important role for the correct formation of ATP-binding pockets.

It should be noted that the above work studies the movements of NBDs without ATP binding. According to ‘ATP Switch model’, it is known that NBDs’ dimerization is induced by the binding of ATP molecules. However, in what extent does the ATP binding induce the dimerization of NBDs, which is not clear currently. How ATP binding to the pocket in IF conformation can induce large conformational changes leading to the IF-OF transition is questionable. Actually, this is an interesting but still open question. Experimentally, fluorescence spectroscopy data have demonstrated that the closing and dimerization of the two NBDs are not only because of the binding of ATP molecules which only causes the limited conformational change (Campbell et al., 2004; Liu & Sharom, 1997; Loo & Clarke, 2000). The mass spectrometry analysis of P-gp (Marcoux et al., 2013) has revealed that the independent binding of nucleotides is not sufficient to induce a significant conformational shift, and the large-scale conformational rearrangement is the result of synergistic binding of lipids, nucleotides and drugs. Additionally, there is no definite experimental result about at which moment of conformational rearrangement ATP molecules bind to the pockets in P-gp. Also, there are some simulation studies (Prajapati et al., 2013; Shahraki et al., 2018b) about the relationship between the ATPase activity and substrate binding, while no definite results have been obtained on what kind of changes happen to NBDs’ structure upon substrate binding, and on how substrate binding makes ATP binding sites transition from a low to a high ATP affinity state. Weng’s group showed the limited conformational changes at NBDs’ interface in the simulation study for ATP-free, ATP-binding and ADP-binding states (Weng et al., 2010). Here, as a drawback of the current work,

ATP molecules and substrates were not included in our study systems. In the future work, we are going to study the question that to what extents the ATP and drug molecule binding results in the conformational transition of human P-gp, respectively.

Conformational transition of the TMDs

In the allosteric process of human P-gp, the TMDs experience large-scale structural rearrangements. In order to describe it, we monitored the changes of the distances between two structurally corresponding TM helices (TM1-TM7, TM2-TM8, TM3-TM9, TM4-TM10, TM5-TM11, and TM6-TM12) respectively in cytoplasmic and periplasmic parts (Figure 3(a) and (b)). As TM1 and TM7 have almost no cytoplasmic parts, only the distance of TM1-TM7 in the periplasmic side was calculated. The monitored 22 residues (2 in each TM helix except for 1 in TM1 and TM7, respectively) forming 11 pair distances are shown in Supplementary Table SI, of which 11 residues are located in periplasmic parts and the other 11 in cytoplasmic parts, and two parts of residues individually have approximately the same z -axis coordinates. From Figure 3(a), the distances between most TM helices in the cytoplasmic side experience a big, almost linear decrease and then become stable since 8.5 ns , while the distances in the periplasmic side nearly maintain a steady value until 7.5 ns and then have a considerable increase (Figure 3(b)). This means that the cytoplasmic parts of TMDs, affected by NBDs, also undergo a closing movement, and not until this movement is almost over do the periplasmic parts of TMDs start to open toward the periplasmic side. The similar result has also been observed in the conformational transition of the *C. elegans* P-gp from OF to IF state by Wang (Wang & Liao, 2015). This means that the periplasmic and cytoplasmic parts of TMD don’t have a chance to be open at the same time, which ensures the unidirectional transport property of P-gp molecule. And it also hints that the closing movement of NBDs is the driving factor for the whole conformational rearrangement of human P-gp, and it is transmitted from the bottom to the top of the system, i.e. from NBDs to the cytoplasmic parts of TMDs, then to the periplasmic parts of TMDs. In addition, interestingly, the P-gp experiences the conformation around 7.5 ns during the Targeted MD simulation in which the two NBDs are dimerized (see Figure 2(a)) and the periplasmic parts of TMDs are still closed (see Figure 3(b)). This conformation might be an outward-occluded state. In 2014, Choudhury et al. resolved the crystal structure of ABC exporter McjD at outward-occluded state (Choudhury et al., 2014). This state represents a transition intermediate between the outward-open and inward-open conformation and has an important role

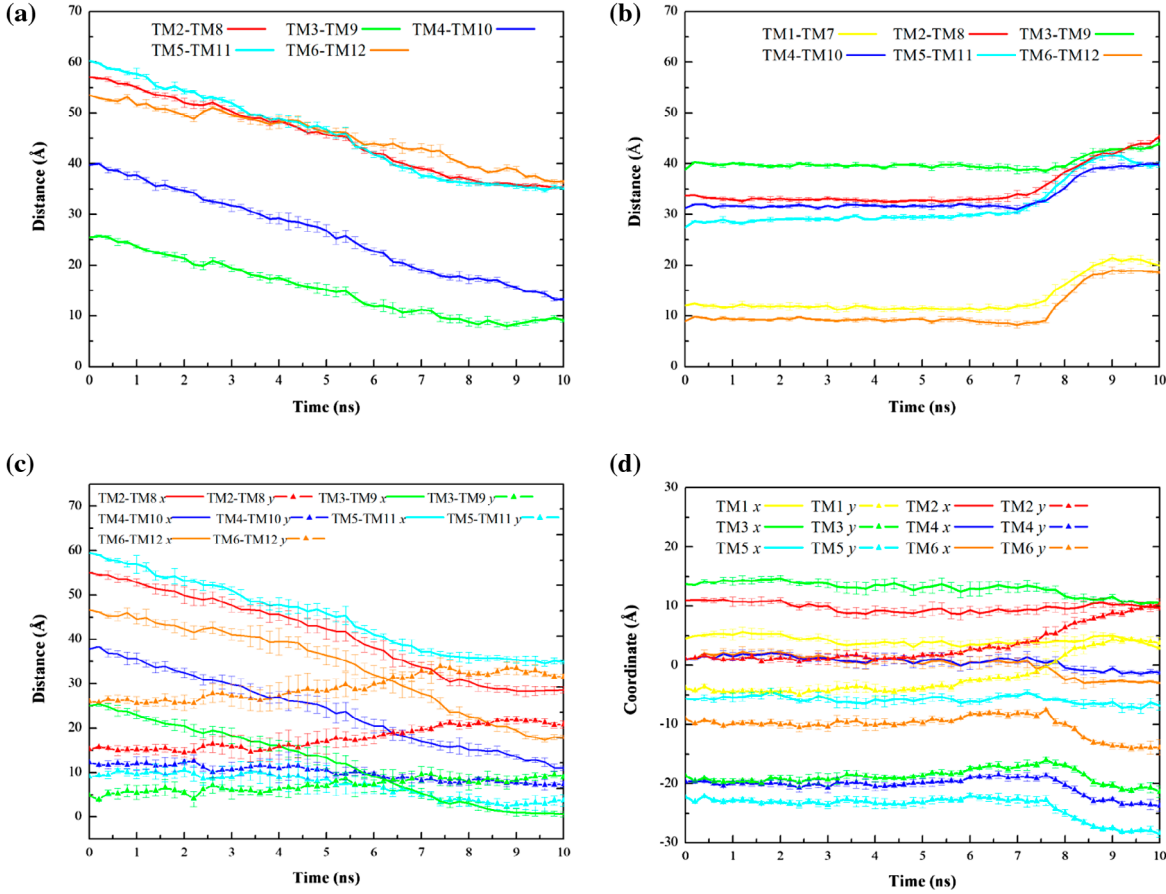


Figure 3. Movements of TM helices. (a) and (b) give the changes of the distances between two structurally corresponding TM helices, respectively in cytoplasmic and periplasmic parts. (c) the distance changes of TM helices' cytoplasmic parts on *x* and *y* directions. (d) the detailed movements of TM helices' periplasmic parts on *x* and *y* directions. The monitored residues (2 in each TM helix, except for 1 in TM1 and TM7 respectively) are shown in Table SI.

for the catalytic and transport cycle of P-gp (Siarheyeva, Liu, & Sharom, 2010).

In order to detect the effect of NBDs' main rotation movements (in *xy* plane) on TM helices' cytoplasmic parts, the movements of TM helices' cytoplasmic parts were decomposed in *x* and *y* directions and the results are shown in Figure 3(c). From Figure 3(c), it is clear that the movements mainly happen in *x* direction. The distance changes of different TM helices' pairs are different, especially in *y* direction, which we think is caused by NBDs' rotation movements. For the movements in *y* direction, the distance change of TM4-TM10 is the least obvious while those of TM6-TM12 and TM2-TM8 are the most, which is understandable with consideration of the rotation coupling between NBDs and TM helices' cytoplasmic parts and the locations of these TM helices: TM4 and TM10 situated almost above the center of NBDs' interface, and TM6 (TM12) and TM2 (TM8) located the most far away from the center axis of NBDs' interface (see Figure S5).

It is important to note that, although the external forces were applied to pull TMs at the periplasmic side to depart from each other, the distances of them at this side remain almost unchanged for the initial long period of time. This demonstrates that the pulling force is a weak perturbation that is not able to change the functional movement of the helices at the periplasmic side. These weak perturbations can thus be used to probe the structural and energetic determinants in the conformational transition.

In addition, we noticed that the opening amplitudes of TM helices toward the periplasmic side are very different. From Figure 3(b), TM2-TM8 and TM5-TM11 have a maximum opening with a distance increase 12 Å, followed by TM4-TM10 and TM1-TM7 about 8 Å, TM6-TM12 5 Å, and TM3-TM9 has a minimum opening with the distance increasing only by 3 Å. Furthermore, we also noticed the differences in the movement directions of TM helices at the periplasmic side. Taking the first half of human P-gp for example, Figure 3(d)

gives the detailed movements of TM helices' periplasmic parts on x and y directions. From Figure 3(d), evidently except that the periplasmic parts of TM1 and TM2 move along positive x and y directions, those parts of other helices including TM3, TM4, TM5 and TM6 move on negative x and y directions. This means that during the reorientation of TM helices, TM1 and TM2 move separately from TM3 and TM6, while they group together in the initial IF state. Here, it should be pointed out that compared with the crystal structure and our modeled one of P-gp in IF state, the O'Mara's OF model has incorrect secondary structures around EL1 region (TM1-EL1-TM2) (see the section of Evaluation of homology modeling of human P-gp in the IF state) because the OF model had been constructed before the P-gp crystal structure was resolved. Thus, the conformational changes during the targeted MD simulation would be accompanied with the folding/unfolding of the region around EL1, which will affect slightly the movements of residues Thr76 and Glu109 we picked to reflect the cytoplasmic part movements of TM1 and TM2. Therefore, the above results about TM1 and TM2 may be of low reliability in some extent. The refinement of the OF model would be favorable. Since this work focused mainly on not ELs but ICLs, such refinement might not affect largely the results presented here. In the future, it is better to refine O'Mara's model or rebuild the OF model using the crystal structure.

From the analyses above, we clarify that the conformational rearrangement of human P-gp is driven by NBDs, and the movements of NBDs are transmitted to the cytoplasmic parts of TMDs, then to the periplasmic parts. Also, the TM helices experience a reorientation and move in different amplitudes, achieving the opening of TMDs towards the periplasmic side. Thus, a question comes up that what on earth causes the reorientation of TM helices (with TM3 and TM6 separating from TM1 and TM2, and grouping together with TM4 and TM5) and their separation from each other in different extent. These questions will be discussed in the following section of Effect of cICLs-NBDs interactions on the reorientation of TM helices.

Movement coupling between NBDs and TMDs

In the preceding sections, we discussed the individual movements of NBDs and TMDs. Since the rearrangement is transmitted from NBDs to TMDs, the movement coupling between them is a critical question needed to be discussed. To this end, we calculated the displacement vector cross-correlation between residues of human P-gp according to formula (2) for the two typical allosteric stages. One stage is from 1 to 5 ns during which both NBDs and cytoplasmic parts of TM helices move close to each other respectively and periplasmic parts of TM

helices have almost no movements, and the other stage is from 7.5 to 9.5 ns during which NBDs and cytoplasmic parts of TM helices nearly complete the closing movements and periplasmic parts of TM helices are experiencing the opening movement (see Figures 2(a) and 3(a) and (b)). For the first typical stage, the conformations were sampled every 0.5 ns and correlation coefficients were computed between two conformations spacing 1 ns, and for the second typical stage, the corresponding values are 0.25 and 0.5 ns, respectively, which produces seven sets of correlation coefficients for every stage. The final cross-correlation map for every stage is the average of seven sets of correlation coefficients on the four simulation trajectories.

Figure 4(a) shows the cross-correlation map of human P-gp for the first typical stage. From Figure 4(a), the two NBDs have a high level of self-correlation and strong negative correlations with each other, which demonstrates again the rigid-body property of each NBD and the opposite movements between the two NBDs. For TMDs, taking TMD1 for example, it is clear that the two helix groups formed respectively by TM1, TM2, TM3, and TM6, and by TM4 and TM5, have intense positive correlations individually and negative correlations with each other, which can be easily explained by the structure of human P-gp: the former group interacting with NBD1 and the latter group with NBD2. In addition, it is noticed that the two ICLs, especially IHs in them, have superior consistence with nearby NBDs (see black boxes in Figure 4(a)), which hints ICLs play an important role in the allosteric transmission from NBDs to TMDs.

Figure 4(b) reflects the cross-correlation map of human P-gp for the second typical stage. In this stage, NBDs almost form dimers and thus they show positive correlations with each other to some extent. For TMDs, also taking TMD1 for example, different from the first typical stage, the TM1 and TM2 helices have negative correlations with the other TM3, TM4, TM5, and TM6 helices, especially for their periplasmic parts (see black boxes in Figure 4(b)), which reflects the reorientation of TM helices and opening movements toward the periplasmic side, consistent with the results in section of Conformational transition of the TMDs. Additionally, the ICLs still have highly positive correlations with the corresponding NBDs.

Based on the analyses above, the TMDs are tightly coupled with NBDs in dynamics through ICLs, especially IHs. The TM helices undergo a rearrangement, resulting in the opening of TMDs to the periplasmic side. The information will help us gain an energy insight into the conformational rearrangement of TM helices in section of Effect of cICLs-NBDs interactions on the reorientation of TM helices.

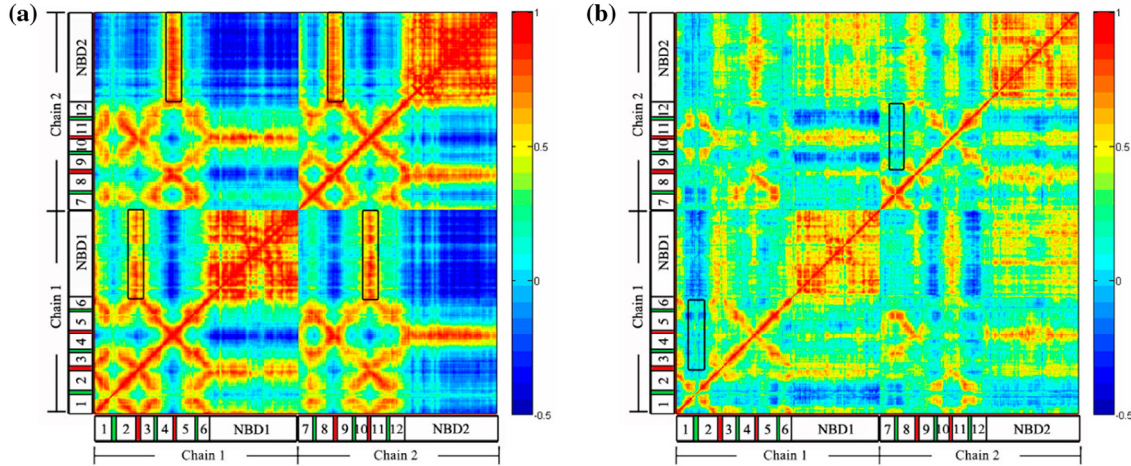


Figure 4. Displacement vector cross-correlation between residues of human P-gp for the two typical allosteric stages. The numbers 1 to 12 represent TM1 to TM12. IHs are colored in red, and ELs in green.

Interface interaction energies between NBDs and TMDs

Since the allosteric signal of human P-gp transmits from NBDs to TMDs, a strong movement coupling exists between NBDs and ICLs, and ICLs were also proposed by Dawson and Locher (2006) to propagate the energy of ATP binding and hydrolysis to the substrate transport, the interaction energy between NBDs and ICLs must play an important role in the allosteric process of human P-gp. The interactions between NBDs and ICLs are non-bond interactions which decay fast with an increasing distance. Therefore, we selected some residues in ICLs which are near NBDs as contact segments (see the section of Materials and Methods) to analyze the interaction energies between NBDs and ICLs. Herein six cICLs were identified with cICL1 (residues 152–172) in ICL1, cICL2 (residues 252–277) in ICL2, cICL3 (residues

793–815) in ICL3, cICL4 (residues 895–920) in ICL4, cICL5 (residues 371–374) and cICL6 (residues 1014–1018) (Figure S6). In fact, we verified the interaction energies between cICLs and NBDs (Figure 5(a)) are almost the same with the interaction energies between ICLs and NBDs (Figure S7). Thus in the energy analyses, the interaction energies between ICLs and NBDs can be represented by the interaction energies between cICLs and NBDs. From Figure 5(a), it is clear that the structurally corresponding cICLs have similar interaction energies with NBDs: cICL1 (cICL3) has about –100 kcal/mol interaction energy with NBD1 (NBD2), cICL4 (cICL2) has approximate –250 kcal/mol interaction energy with NBD1 (NBD2), and cICL5 (cICL6) has about –30 kcal/mol interaction energy with NBD1 (NBD2) in most time of simulations. The differences in the interaction energies between cICLs and NBDs are

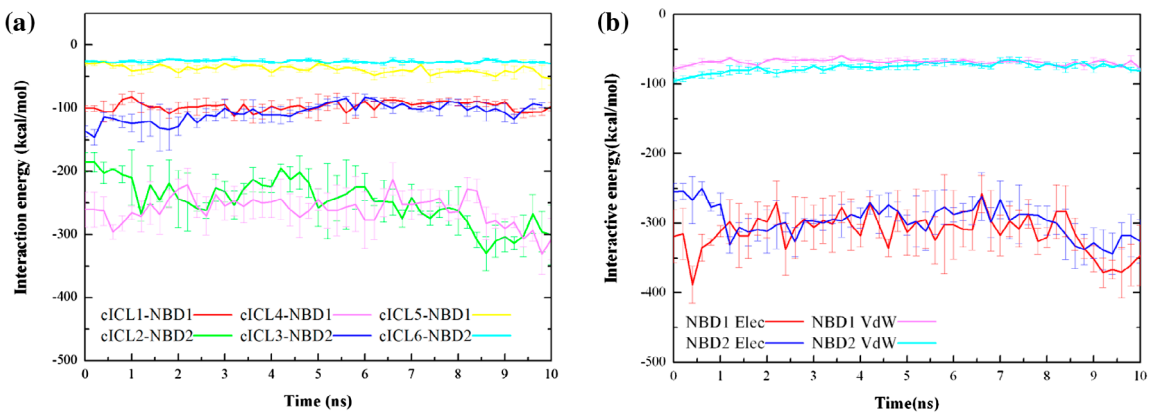


Figure 5. Interaction energies between NBDs and cICLs (a) and the electrostatic (Ele) and van der Waals (vdW) energies between NBD1 and cICL1, cICL4 and cICL5, and between NBD2 and cICL2, cICL3 and cICL6 (b).

mainly caused by the different position relationship between them. According to the structure of human P-gp (Figure S6), cICL2 and cICL4 are closer than cICL1 and cICL3 to the corresponding adjacent NBDs, which makes the former have larger interaction energies than the latter with corresponding NBDs. In addition, we found that the electrostatic interaction energies are much higher than the van der Waals interaction energies between cICLs and NBDs (Figure 5(b)), which means that the electrostatic interactions play an important role for the allosteric signal transmission from NBDs to TMDs. Here, comes another question that whether or not there are some relationships between the cICLs-NBDs different interactions and the conformational rearrangement of human P-gp, which will be discussed in section of Effect of cICLs-NBDs interactions on the reorientation of TM helices. How the energy is transmitted from NBDs to the periplasmic part of TMDs is an interesting question and important for us to understand mechanically the rearrangement of the P-gp. This will be our future work.

Effect of cICLs-NBDs interactions on the reorientation of TM helices

In the preceding sections, two questions have come up. The first one is why TM3 and TM6 helices move away from the TM1 and TM2 helices, finally resulting in the opening of TMDs toward the periplasmic side, and additionally why the different structurally corresponding TM helix pairs separate from each other to different extent in the periplasmic side. Another question is whether the differences in interaction energies between cICLs and NBDs are of great significance for the conformational

rearrangement of human P-gp. The answers to these questions are very important for us to understand the mechanisms of the rearrangement of human P-gp. In the following part, still taking the first half of human P-gp for example, we will try to explain and answer these questions based on the information about the movement directions of TM helices and the interaction energies between cICLs and NBDs. According the movement coupling between NBDs and TMDs, it is known that cICL1 and cICL5, coupled with NBD1, move along negative x and y directions, while cICL2, coupled with NBD2, moves in positive x and y directions. Generally for an independent TM helix, it will tilt to the opposite direction dragged by its bottom cICL. Thus we speculate that the periplasmic parts of TM1, TM2, TM3, and TM6 should move along positive x and y axes, i.e. opposite to the movement directions of cICL1 and cICL5, and the periplasmic parts of TM4 and TM5 should move on the negative x and y axes, contrary to the movement direction of cICL2. However, the fact is that except for TM1, TM2, TM4, and TM5, the movement directions of TM3 and TM6 are not like what we speculate above, but along negative x and y axes (Figure 6). Combining the information on the movement directions of periplasmic parts of TM helices (Figure 3(d)) and the differences in the interaction energies between cICLs and NBDs (Figure 5(a)), we think that the differences in the interaction energies between cICLs and NBDs play an important role for the real movement directions of TM3 and TM6 contrary to our speculation. In the real structure, the movement of every TM helix will be affected by energies from not only the bottom cICL connected directly with it, but also from the cICL connected with it through the EL and a TM helix (Figure 6). For TM1 and TM2,

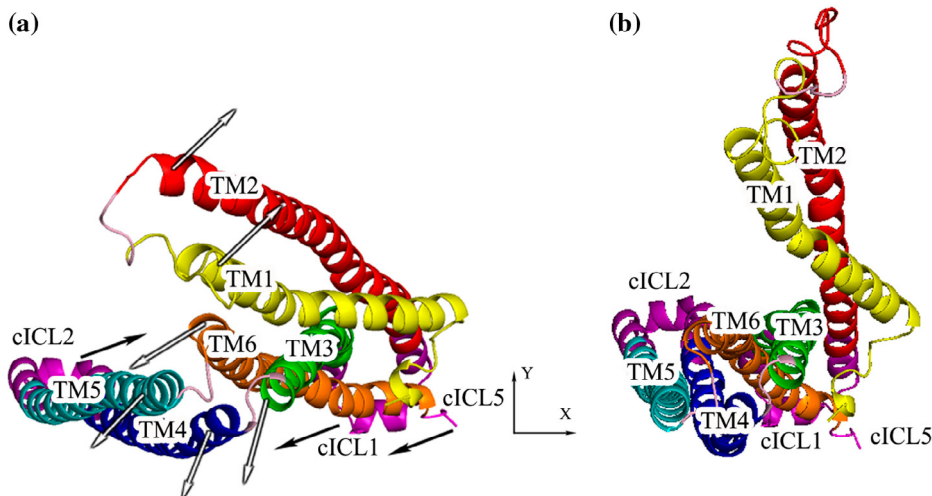


Figure 6. TMD1 at the initial inward-facing conformation (a) and the final outward-facing conformation (b). Black filled arrows represent the movement directions of cICLs and black hollow arrows show the movement directions of periplasmic parts of TM helices.

the energies affecting their movements come only from cICL1, while for other TM helices, the situations are more complicated. For example, the energies affecting the movement of TM3 come from its bottom cICL1 which makes TM3 move along x and y positive directions, and cICL2 connected with TM3 through TM4 and EL which makes TM4, also TM3 move along negative x and y directions. From Figure 5(a), we know the interaction energy between NBD2 and cICL2 (-250 kcal/mol) is much bigger than that between NBD1 and cICL1 (-100 kcal/mol). Therefore, the movement of TM3 is dominantly controlled by the energy from cICL2, which finally leads TM3 to move on x and y negative directions. The movement directions of other TM helices can also be explained in the similar way.

Additionally, it should be pointed out that the differences in the interaction energies between cICLs and NBDs also influence the movement amplitudes of TM helices. For example, according to the data in Figure 3(d), the periplasmic parts of TM4 and TM5 almost with the same z coordinates, have different movement amplitudes along negative x and y directions with the latter much bigger than the former. According to the structure of human P-gp, the energies affecting the movement of TM5 come from the energy difference between cICL2-NBD2 (-250 kcal/mol) and cICL5-NBD1 (-30 kcal/mol) which is much bigger than the energy difference between cICL1-NBD1 (-100 kcal/mol) and cICL2-NBD2 (-250 kcal/mol) which mainly affects the movement of TM4. That is why the periplasmic part of TM5 moves much farther than that of TM4.

Through the analyses above, we can conclude that the subtle differences in the interaction energies between cICLs (ICLs) with NBDs play an important role in leading the periplasmic parts of TM helices to open toward the periplasmic side along the established directions and in the appropriate amplitudes, achieving the conformational rearrangement of human P-gp from the inward- to outward-facing states. The tight energy coupling between

cICLs (ICLs) and NBDs ensures the coordinated operation of the allosteric process of human P-gp.

Explanation of the cross-linking and residue mutation experimental phenomena

In order to further indicate the importance of the cICLs-NBDs different interactions for NBDs in controlling the opening of the periplasmic parts of TM helices along the established directions and in the appropriate amplitudes, here we try to explain some experimental phenomena through this energy point of view proposed above. Loo and Clarke (2015) have confirmed that both IH1/IH4 and IH2/IH3 cross-linking can severely inhibit the activity of human P-gp to transport substrates. According to this energy point of view, in the situation of the cross-linking of IH1 and IH4, the energies affecting the movement of TM3 changes from the energy difference between cICL1-NBD1 (-100 kcal/mol) and cICL2-NBD2 (-250 kcal/mol) to the energy difference between the sum of cICL1-NBD1 (-100 kcal/mol) and cICL4-NBD1 (-250 kcal/mol) and cICL2-NBD2 (-250 kcal/mol). Evidently, the cICLs controlling dominantly the movement of TM3 changes from cICL2 to cICL1, which will change the movement direction of TM3 from negative x and y directions to positive x and y directions. Thus, TM3 will not separate from TM1 and TM2, leading the periplasmic parts of TM helices cannot open correctly and furtherly the substrates cannot be released effectively. The activity inhibition of human P-gp caused by the cross-linking of IH2/IH3 can also be explained in the similar way.

Additionally, Loo and Clarke (2015) have also confirmed that the mutant R262A and R905A at the same time will maintain 70% of P-gp ATPase activity. To explain this phenomenon, first we calculated the interaction energies between every residue in IH2 (IH4) and NBD2 (NBD1) (Figure 7). From Figure 7, it is clear that the interaction energies of residues in IH4 with NBD1

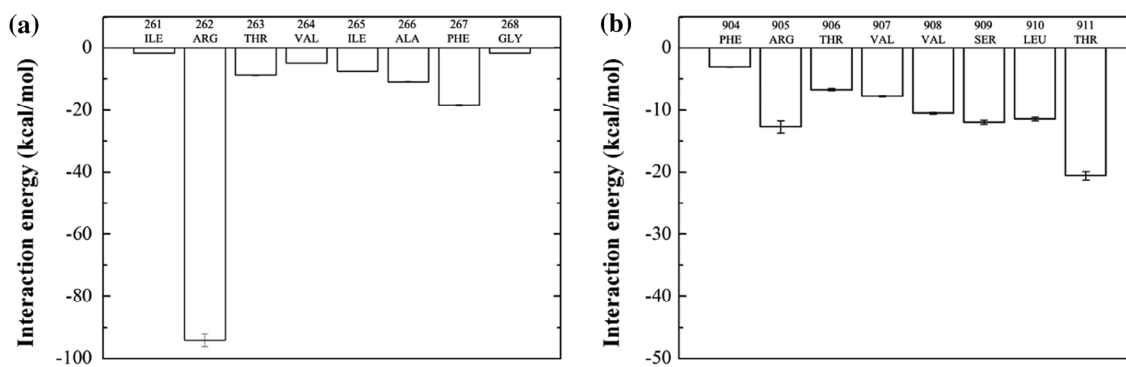


Figure 7. Interaction energies between the residues in IH2 and NBD2 (a), and between the residues in IH4 and NBD1 (b).

are approximately equal, while for IH2, the interaction energy between Arg262 and NBD2 is dominant, which has also been found in the simulation by Chang et al. (2013), demonstrating that Arg262 plays an important role in the interaction energy between cICL2 and NBD2. Arg262 is a positively charged amino acid residue, and it has a tight contact with a negatively charged residue Glu1084 situated in NBD2 (about 1.6–1.8 Å between the nearest atoms including hydrogen atoms respectively from Arg262 and Glu1084 during the simulation), while Arg905 is about 6.8–9.8 Å apart from the nearest negatively charged residue Glu476 located in NBD1. This may partially contribute to the reason why Arg262 has a stronger electrostatic interaction with NBD2 than Arg905 with NBD1. The mutant R262A means the interaction energy between residue 262 and NBD2 will decrease from –95 kcal/mol to approximately –10 kcal/mol (taking the interaction energy between Ala266 and NBD2 as an approximation), which will cause the interaction energy between cICL2 and NBD2 to reduce by about 85 kcal/mol, from –250 to –165 kcal/mol. Thus, the interaction energy between cICL2 and NBD2 is still larger than that between cICL1 and NBD1 (–100 kcal/mol), but their difference becomes smaller to some extent. Therefore, the movement amplitudes of TM3, TM4, TM5 and TM6 will decrease, which hints TMD1 cannot completely open. From Figure 7(b), the mutant R905A will have a minor impact on the interaction energy between cICL4 and NBD1, and thus the movement amplitudes of the periplasmic parts of the helices in TMD2 will have nearly no changes. Based on the analyses above, the mutant R262A and R905A at the same time will only affect the movement amplitudes of the first half of human P-gp, and therefore the effects of the mutant R262A and R905A at the same time decrease the activity of human P-gp to some extent.

It should be pointed out that so far consistent conclusions have not been obtained about the importance of Arg262 (in IH2) and Arg905 (in IH4) in the P-gp ATPase activity. Pajeva et al. predicted that both of them are critical for coupling ATP hydrolysis to drug efflux based on the equilibrium MD simulation (Pajeva, Hanl, & Wiese, 2013), while our and Chang et al.'s works gave that Arg262 is important but Arg905 is not through the targeted MD simulations (Chang et al., 2013). Experimentally, Loo et al. found that both mutants (R262A/R905A and T263A/T906A) retained about 70% of wild-type verapamil stimulated ATPase activity (Loo & Clarke, 2015). Based on the above results, we think that compared with Arg905, Arg262 may be more important. The reason for the decrease of ATPase activity for the mutant R262A/R905A probably mainly comes from R262A mutation. The decline of the ATPase activity in the mutant T263A/T906A maybe lies in the effect of T263A mutation on Arg262's side chain and further its

interaction with Glu1084, which will result in almost the same degree of decrease in the ATPase activity with the mutant R262A/R905A. The above analysis is only our speculation, and further experiments should be done to demonstrate the importance of Arg262 in IH2 and Arg905 in IH4 in the P-gp ATPase activity.

These two experimental phenomena about the cross-linking and residue mutations can be explained by our energy point of view. This indicates that the differences in the cICLs (ICLs)-NBDs interaction energies are likely to play an important role for human P-gp transition from the inward- to outward-facing states. More structural and biochemical evidences are needed to validate this point in the future.

Additionally, protein rearrangement generally takes place on the time scale of microseconds or milliseconds, or even longer. Therefore, the 10 ns targeted MD simulation of human P-gp transition in this work is of time scale limitations. And this will be overcome as the computational power increases in the future. Though, the consistency of our results with some experimental and other theoretical data hints that the results about the movement and energy aspects are of reasonability to some extent and are helpful for understanding the physical mechanism of human P-gp conformational transition.

Conclusions

In this study, the conformational rearrangement of human P-gp has been simulated from inward- to outward-facing states using targeted MD simulations. The human P-gp inward-facing model is constructed through homology modeling using the structure of mouse P-gp as the template. The quality of the model is checked by Ramachandran plot, and over 99% residues are in the acceptable regions, indicating this model can be utilized in the targeted MD simulations. It's found that in the allosteric progress, the NBDs have not only a translation movement, but also a rotation movement between them. The rotation movement mainly happens in *xy* plane and ensures the two ATP-binding pockets form correctly. The rearrangement is driven by NBDs, and the signal is transmitted from NBDs to the cytoplasmic parts of TMDs, and finally to the periplasmic parts. In this process, the TM helices undergo a reorientation. To account for this phenomenon, six structure segments cICLs have been identified and the energy analyses confirm that the interaction energies between cICLs and NBDs can represent those between ICLs and NBDs. The further analyses on the relationship between the movements of TM helices and the interaction energies between cICLs and NBDs come to a conclusion that the subtle differences in the interaction energies between cICLs and NBDs plays an important role in leading the periplasmic parts of TM helices to open along the established directions and in

the appropriate amplitudes, achieving the reorientation of TMDs. The tightly energy and dynamic coupling between cICLs and NBDs ensures largely the coordinated operation of the allosteric process of human P-gp. This energy insight can explain two experimental phenomena about the cross-linking and residue mutations. Our results give allosteric details and an energy insight into the conformational rearrangement of human P-gp.

Supplementary material

The supplemental material for this article is available at <http://doi.org/10.1080/07391102.2018.1461133>.

Disclosure statement

No potential conflict of interest was reported by the authors.

Funding

This work was supported in part by grants from the National Natural Science Foundation of China [grant number 11474013]; the Natural Science Foundation of Beijing [grant number 4152011].

References

- Binkhathlan, Z., & Lavasanifar, A. (2013). P-glycoprotein inhibition as a therapeutic approach for overcoming multidrug resistance in cancer: Current status and future perspectives. *Curr Cancer Drug Targets*, 13, 326–346.
- Bera, K., Rani, P., Kishor, G., Agarwal, S., Kumar, A., & Singh D. V. (2017) Structural elucidation of transmembrane domain zero (TMD0) of EcdL: A multidrug resistance-associated protein (MRP) family of ATP-binding cassette transporter protein revealed by atomistic simulation. *Journal of Biomolecular Structure and Dynamics* 1–13.
- Campbell, J. D., Deol, S. S., Ashcroft, F. M., Kerr, I. D., & Sansom, M. S. (2004). Nucleotide-dependent conformational changes in HisP: Molecular dynamics simulations of an ABC transporter nucleotide-binding domain. *Biophysical Journal*, 87, 3703–3715.
- Chang, S. Y., Liu, F. F., Dong, X. Y., & Sun, Y. (2013). Molecular insight into conformational transmission of human P-glycoprotein. *The Journal of Chemical Physics*, 139, 225102.
- Chen, C. J., Chin, J. E., Ueda, K., Clark, D. P., Pastan, I., Gottesman, M. M., & Roninson, I. B. (1986). Internal duplication and homology with bacterial transport proteins in the mdr1 (P-glycoprotein) gene from multidrug-resistant human cells. *Cell*, 47, 381–389.
- Chen, J., Lu, G., Lin, J., Davidson, A. L., & Quiocho, F. A. (2003). A tweezers-like motion of the ATP-binding cassette dimer in an ABC transport cycle. *Molecular Cell*, 12, 651–661.
- Choudhury, H. G., Tong, Z., Mathavan, I., Li, Y., Iwata, S., Zirah, S., ... Beis, K. (2014). Structure of an antibacterial peptide ATP-binding cassette transporter in a novel outward occluded state. *Proceedings of the National Academy of Sciences*, 111, 9145–9150.
- Compoint, M., Picaud, F., Ramseyer, C., & Girardet, C. (2005). Targeted molecular dynamics of an open-state KcsA channel. *The Journal of Chemical Physics*, 122, 134707.
- Dawson, R. J., & Locher, K. P. (2006). Structure of a bacterial multidrug ABC transporter. *Nature*, 443, 180–185.
- Dwivedi, GR., Tyagi, R., Sanchita, Tripathi, S., Pati, S., Srivastava, SK., ... Sharma, A. (2018) Antibiotics potentiating potential of catharanthine against superbug *Pseudomonas aeruginosa*. *Journal of Biomolecular Structure and Dynamics*, 1–15.
- Eckford, P. D., & Sharom, F. J. (2009). ABC efflux pump-based resistance to chemotherapy drugs. *Chemical Reviews*, 109, 2989–3011.
- Essmann, U., Perera, L., Berkowitz, M. L., Darden, T., Lee, H., & Pedersen, L. G. (1995). A smooth particle mesh Ewald method. *The Journal of Chemical Physics*, 103, 8577–8593.
- Eswar, N., Eramian, D., Webb, B., Shen, M. Y., & Sali, A. (2008). Protein structure modeling with MODELLER. *Methods in Molecular Biology*, 426, 145–159.
- Feller, S. E., Yin, D., Pastor, R. W., & MacKerell, A. J. (1997). Molecular dynamics simulation of unsaturated lipid bilayers at low hydration: Parameterization and comparison with diffraction studies. *Biophysical Journal*, 73, 2269–2279.
- Furuta, T., Yamaguchi, T., Kato, H., & Sakurai, M. (2014). Analysis of the structural and functional roles of coupling helices in the ATP-binding cassette transporter MsbA through enzyme assays and molecular dynamics simulations. *Biochemistry*, 53, 4261–4272.
- Gekeler, V., Weger, S., & Probst, H. (1990). Mdr1P-glycoprotein gene segments analyzed from various human leukemic cell lines exhibiting different multidrug resistance profiles. *Biochemical and Biophysical Research Communications*, 169, 796–802.
- Gutmann, D. A., Ward, A., Urbatsch, I. L., Chang, G., & van Veen, H. W. (2010). Understanding polyspecificity of multidrug ABC transporters: Closing in on the gaps in ABCB1. *Trends in Biochemical Sciences*, 35, 36–42.
- Higgins, C. F., & Linton, K. J. (2004). The ATP switch model for ABC transporters. *Nature Structural & Molecular Biology*, 11, 918–926.
- Hoover, W. G. (1985). Canonical dynamics: Equilibrium phase-space distributions. *Physical Review A*, 31, 1695–1697.
- Humphrey, W., Dalke, A., & Schulten, K. (1996). VMD: Visual molecular dynamics. *Journal of Molecular Graphics*, 14(33–38), 27–28.
- Ichijo, T., & Karplus, M. (1991). Collective motions in proteins: A covariance analysis of atomic fluctuations in molecular dynamics and normal mode simulations. *Proteins: Structure, Function, and Genetics*, 11, 205–217.
- Kamerlin, S., Rucker, R., & Boresch, S. (2006). A targeted molecular dynamics study of WPD loop movement in PTP1B. *Biochemical & Biophysical Research Communications*, 345, 1161–1166.
- Katayama, K., Kapoor, K., Ohnuma, S., Patel, A., Swaim, W., Ambudkar, I. S., & Ambudkar, S. V. (2015). Revealing the fate of cell surface human P-glycoprotein (ABCB1): The lysosomal degradation pathway. *Biochimica et Biophysica Acta (BBA) – Molecular Cell Research*, 1853, 2361–2370.
- Kesherwani, M., Michael, G. M., Fukui, K., & Velmurugan, D. (2017). Identification of novel natural inhibitor for NorM – A multidrug and toxic compound extrusion transporter – An insilico molecular modeling and simulation studies.

- Journal of Biomolecular Structure and Dynamics*, 35, 58–77.
- Kioka, N., Tsubota, J., Kakehi, Y., Komano, T., Gottesman, M. M., Pastan, I., & Ueda, K. (1989). P-Glycoprotein gene (MDR1) cDNA from human adrenal: Normal P-glycoprotein carries Gly185 with an altered pattern of multidrug resistance. *Biochemical and Biophysical Research Communications*, 162, 224–231.
- Klepsch, F., & Ecker, G. F. (2010). Impact of the recent mouse P-glycoprotein structure for structure-based ligand design. *Molecular Informatics*, 29, 276–286.
- Kolaskar, A. S., & Sawant, S. (1996). Prediction of conformational states of amino acids using a Ramachandran plot. *International Journal of Peptide and Protein Research*, 47, 110–116.
- Kong, Y., Ma, J., Karplus, M., & Lipscomb, W. N. (2006). The allosteric mechanism of yeast chorismate mutase: A dynamic analysis. *Journal of Molecular Biology*, 356, 237–247.
- Kort, A., Sparidans, R. W., Wagenaar, E., Beijnen, J. H., & Schinkel, A. H. (2015). Brain accumulation of the EML4-ALK inhibitor ceritinib is restricted by P-glycoprotein (P-GP/ABCB1) and breast cancer resistance protein (BCRP/ABCG2). *Pharmacological Research*, 102, 200–207.
- Laskowski, R. A., MacArthur, M. W., Moss, D. S., & Thornton, J. M. (1993). PROCHECK: A program to check the stereochemical quality of protein structures. *Journal of Applied Crystallography*, 26, 283–291.
- Linton, K. J., & Higgins, C. F. (2007). Structure and function of ABC transporters: The ATP switch provides flexible control. *Pflügers Archiv – European Journal of Physiology*, 453, 555–567.
- Liu, R., & Sharom, F. J. (1997). Fluorescence studies on the nucleotide binding domains of the P-glycoprotein multidrug transporter. *Biochemistry*, 36, 2836–2843.
- Locher, K. P. (2008). Structure and mechanism of ATP-binding cassette transporters. *Philosophical Transactions of the Royal Society B Biological Sciences*, 364, 239–245.
- Lomize, M. A., Lomize, A. L., Pogozheva, I. D., & Mosberg, H. I. (2006). OPM: Orientations of proteins in membranes database. *Bioinformatics*, 22, 623–625.
- Loo, T. W., & Clarke, D. M. (2000). Identification of residues within the drug-binding domain of the human multidrug resistance P-glycoprotein by cysteine-scanning mutagenesis and reaction with dibromobimane. *Journal of Biological Chemistry*, 275, 39272–39278.
- Loo, T. W., & Clarke, D. M. (2008). Mutational analysis of ABC proteins. *Archives of Biochemistry & Biophysics*, 476, 51–64.
- Loo, T. W., & Clarke, D. M. (2015). The transmission interfaces contribute asymmetrically to the assembly and activity of human P-glycoprotein. *Journal of Biological Chemistry*, 290, 16954–16963.
- Ma, J., Sigler, P. B., Xu, Z., & Karplus, M. (2000). A dynamic model for the allosteric mechanism of GroEL. *Journal of Molecular Biology*, 302, 303.
- MacKerell, A. D., Bashford, D., Bellott, M., Dunbrack, R. L., Evanseck, J. D., Field, M. J., ... Karplus, M. (1998). All-atom empirical potential for molecular modeling and dynamics studies of proteins. *The Journal of Physical Chemistry B*, 102, 3586–3616.
- Manoharan, P., Chennouj, K., & Ghoshal, N. (2018). Computational analysis of BACE1-ligand complex crystal structures and linear discriminant analysis for identification of BACE1 inhibitors with anti P-glycoprotein binding property. *Journal of Biomolecular Structure and Dynamics*, 36, 262–276.
- Manoharan, P., & Ghoshal, N. (2017). Fragment-based virtual screening approach and molecular dynamics simulation studies for identification of BACE1 inhibitor leads. *Journal of Biomolecular Structure and Dynamics*, 1–15.
- Marcoux, J., Wang, S. C., Politis, A., Reading, E., Ma, J., Biggin, P. C., ... Robinson, C. V. (2013). Mass spectrometry reveals synergistic effects of nucleotides, lipids, and drugs binding to a multidrug resistance efflux pump. *Proceedings of the National Academy of Sciences*, 110, 9704–9709.
- Matsson, P., Pedersen, J. M., Norinder, U., Bergström, C. A. S., & Artursson, P. (2009). Identification of novel specific and general inhibitors of the three major human ATP-binding cassette transporters P-gp, BCRP and MRP2 among registered drugs. *Pharmaceutical Research*, 26, 1816–1831.
- McCormick, J. W., Vogel, P. D., & Wise, J. G. (2015). Multiple drug transport pathways through human P-glycoprotein. *Biochemistry*, 54, 4374–4390.
- Moradi, M., & Tajkhorshid, E. (2013). Mechanistic picture for conformational transition of a membrane transporter at atomic resolution. *Proceedings of the National Academy of Sciences*, 110, 18916–18921.
- Mornon, J. P., Lehn, P., & Callebaut, I. (2008). Atomic model of human cystic fibrosis transmembrane conductance regulator: Membrane-spanning domains and coupling interfaces. *Cellular and Molecular Life Sciences*, 65, 2594–2612.
- Nosé, S. (1984). A unified formulation of the constant temperature molecular dynamics methods. *The Journal of Chemical Physics*, 81, 511–519.
- O'Mara, M. L., & Tielemans, D. P. (2007). P-glycoprotein models of the apo and ATP-bound states based on homology with Sav1866 and MalK. *FEBS Letters*, 581, 4217–4222.
- Pajeva, I. K., Hanl, M., & Wiese, M. (2013). Protein contacts and ligand binding in the inward-facing model of human P-glycoprotein. *ChemMedChem*, 8, 748–762.
- Pan, L., & Aller, S. G. (2015). Equilibrated atomic models of outward-facing P-glycoprotein and effect of ATP binding on structural dynamics. *Scientific Reports*, 5, 555.
- Pandey, B., Grover, S., Tyagi, C., Goyal, S., Jamal, S., Singh, A., ... Grover, A. (2018). Dynamics of fluoroquinolones induced resistance in DNA gyrase of *Mycobacterium tuberculosis*. *Journal of Biomolecular Structure and Dynamics*, 36, 362–375.
- Phillips, J. C., Braun, R., Wang, W., Gumbart, J., Tajkhorshid, E., Villa, E., ... Schulten, K. (2005). Scalable molecular dynamics with NAMD. *Journal of Computational Chemistry*, 26, 1781–1802.
- Prajapati, R., & Sangamwar, A. T. (2014). Translocation mechanism of P-glycoprotein and conformational changes occurring at drug-binding site: Insights from multi-targeted molecular dynamics. *Biochimica et Biophysica Acta (BBA) – Biomembranes*, 1838, 2882–2898.
- Prajapati, R., Singh, U., Patil, A., Khomane, K. S., Bagul, P., Bansal, A. K., & Sangamwar, A. T. (2013). *In silico* model for P-glycoprotein substrate prediction: Insights from molecular dynamics and *in vitro* studies. *Journal of Computer-Aided Molecular Design*, 27, 347–363.
- Sanchez, R., & Sali, A. (2000). Comparative protein structure modeling. Introduction and practical examples with modeller. *Methods in Molecular Biology*, 143, 97–129.
- Sauna, Z. E., & Ambudkar, S. V. (2007). About a switch: How P-glycoprotein (ABCB1) harnesses the energy of ATP binding and hydrolysis to do mechanical work. *Molecular Cancer Therapeutics*, 6, 13–23.

- Schlitter, J., Engels, M., Krüger, P., Jacoby, E., & Wollmer, A. (1993). Targeted molecular dynamics simulation of conformational change-application to the T ↔ R transition in insulin. *Molecular Simulation*, *10*, 291.
- Seeger, M. A., & van Veen, H. W. (2009). Molecular basis of multidrug transport by ABC transporters. *Biochimica et Biophysica Acta (BBA) – Proteins and Proteomics*, *1794*, 725–737.
- Shahraki, O., Zargari, F., Edraki, N., Khoshneviszadeh, M., Firuzi, O., & Miri, R. (2018a). Molecular dynamics simulation and molecular docking studies of 1,4-Dihydropyridines as P-glycoprotein's allosteric inhibitors. *Journal of Biomolecular Structure and Dynamics*, *36*, 112–125.
- Shahraki, O., Zargari, F., Edraki, N., Khoshneviszadeh, M., Firuzi, O., & Miri, R. (2018b). Molecular dynamics simulation and molecular docking studies of 1,4-Dihydropyridines as P-glycoprotein's allosteric inhibitors. *Journal of Biomolecular Structure and Dynamics*, *36*, 112–125.
- Shen, M. Y., & Sali, A. (2006). Statistical potential for assessment and prediction of protein structures. *Protein Science*, *15*, 2507–2524.
- Siarheyeva, A., Liu, R., & Sharom, F. J. (2010). Characterization of an asymmetric occluded state of P-glycoprotein with two bound nucleotides: Implications for catalysis. *Journal of Biological Chemistry*, *285*, 7575–7586.
- Smith, P. C., Karpowich, N., Millen, L., Moody, J. E., Rosen, J., Thomas, P. J., & Hunt, J. F. (2002). ATP binding to the motor domain from an ABC transporter drives formation of a nucleotide sandwich dimer. *Molecular Cell*, *10*, 139–149.
- ter Beek, J., Guskov, A., & Slotboom, D. J. (2014). Structural diversity of ABC transporters. *The Journal of General Physiology*, *143*, 419–435.
- Tsujimura, S., Saito, K., Nawata, M., Nakayamada, S., & Tanaka, Y. (2008). Overcoming drug resistance induced by P-glycoprotein on lymphocytes in patients with refractory rheumatoid arthritis. *Annals of the Rheumatic Diseases*, *67*, 380–388.
- Vangunsteren, W. F., & Berendsen, H. (1977). Algorithms for macromolecular dynamics and constraint dynamics. *Molecular Physics*, *34*, 1311–1327.
- Wang, H., Hong, W., Paterson, I. C., Pu, J., & Laughon, C. A. (2014). Identification of the PcrA DNA helicase reaction pathway by applying advanced targeted molecular dynamic simulations. *Molecular Simulation*, *40*, 1290–1299.
- Wang, Z., & Liao, J. L. (2015). Probing structural determinants of ATP-binding cassette exporter conformational transition using coarse-grained molecular dynamics. *The Journal of Physical Chemistry B*, *119*, 1295–1301.
- Weng, J. W., Fan, K. N., & Wang, W. N. (2010). The conformational transition pathway of ATP binding cassette transporter MsbA revealed by atomistic simulations. *Journal of Biological Chemistry*, *285*, 3053–3063.
- Wise, J. G. (2012). Catalytic transitions in the human MDR1 P-glycoprotein drug binding sites. *Biochemistry*, *51*, 5125–5141.
- Xiao, X., Zeng, X., Yuan, Y., Gao, N., Guo, Y., Pu, X., & Li, M. (2015). Understanding the conformation transition in the activation pathway of β2 adrenergic receptor via a targeted molecular dynamics simulation. *Physical Chemistry Chemical Physics*, *17*, 2512–2522.
- Zhong, W., & Guo, W. (2009). Mixed modes in opening of KcsA potassium channel from a targeted molecular dynamics simulation. *Biochemical & Biophysical Research Communications*, *388*, 86–90.